2024 IEEE/RSJ International Conference on Intelligent Robots and Systems (IROS)
October 14-18, 2024. Abu Dhabi, UAE

Importance of Translational Velocity for Bird-scale Flapping Wing Vehicles Incapable of Hovering

Shijun Zhou, Aidan Orr and Nak-Seung P. Hyun*

***Abstract*— There exist multiple types of flyers in the world that either achieve lift through leveraging aerodynamics by cleverly choosing the wing airfoils of an airplane, or by flapping their wings. As the flapping wing vehicles (FWVs) decrease in scale, lift is predominantly generated by flapping. However, bigger birds or bird-scale flapping wing vehicle (BFWV) may not be able to hover but leverage the forward velocity to augment the lift generation. In this paper, we analyze the aerodynamic lift augmentation through the translational velocity for a 12g, BFWV with tail (flapping around 14 Hz). We prove that the vehicle is unable to hover, but there exist a significant augmentation through the translational motion. A cycle-averaged aerodynamic model including the contribution from the translational velocity is proposed, and experimentally validated. Finally, the analysis of the sufficient conditions on the velocity direction and orientation are studied to maintain the zero angular moment forward flight.**

I. INTRODUCTION

In nature, birds and insects flap their wings to robustly navigate through challenging environments (e.g., strong winds and clustered forests). The challenge in designing and manufacturing a bio-inspired flapping wing vehicle (FWV) is to ensure sufficient lift force generation while minimizing its weight. Researchers have been able to design and manufacture insect-scale FWV as light as 80-mg [1], [2]. These insect-scale FWVs use piezoelectric actuators to reduce the weight and provide enough power to oscillate their wings at higher frequencies (e.g., Harvard Robobee flapping at 160 Hz). The FWV's high flapping frequency allows the vehicle to hover. At a relatively larger scale with a slower flapping frequency, many researchers have successfully demonstrated hovering flights inspired by the Hummingbird [3]. The common feature among these FWVs lies in the capability of hovering [4].

However, not every animal that flies can hover by flapping. As the size of the flyer decreases, the flapping frequency increases. On the other hand, larger animals with lower flapping frequency can not hover but can instead, move extremely fast laterally [15]. Therefore, the hovering capability can be used as a criterion to distinguish between two different types of FWVs: hovering and translational flyers. We surveyed literatures that demonstrated the flight maneuvers of FWVs based on their operational Reynolds number regime, flapping frequency, and total weight in Fig. 1. The triangles represent the FWVs, which demonstrates the hovering flight, and we denote it as *a hovering flyer*. The circles represent

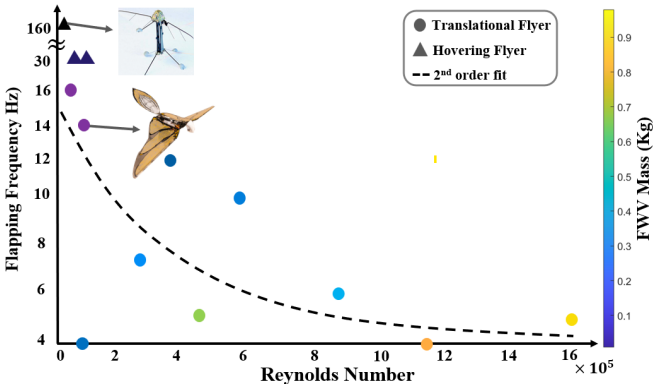

Fig. 1. Flapping frequency versus Reynolds number across a range of FWV of various masses; low Reynolds number regime is dominated by hovering flyers and smaller BFWVs with higher flapping frequency ($\geq$ 14 Hz), while the larger translational flyers on the scale of seagulls with lower flapping frequencies ($\leq$ 10 Hz) occupy the higher Reynolds number regime. Flyers referenced in the figure: [5]–[14]

the FWVs, which demonstrate only the translational motions, and we denote it as *a translational flyer*. The hovering flyers tend to flap their wings at higher frequencies, and the weights are relatively less than the translational flyers. Fig. 1 captures the strong correlation between flapping frequency and Reynolds number which demonstrates translational flyers' ability to traverse translationally at higher speeds.

In addition, the translational flyers often have the flying characteristics of the larger avians that incorporates both flapping and gliding during forward flights. This allows them to conserve energy while taking full advantage of leading edge vortex (LEV) generated during both flapping and gliding [16], [17]. As demonstrated in the translational flight of the Indian leaf butterfly with an average wing span of 65mm, the aerodynamic forces it generates are directly proportional to its forward flight speed and underestimating the flight speed may lead to an underestimation of its thrust generation [18]. Inspired by translational flyers' different modes of flight, we postulate a hybrid lift generation approach within the translational flyer class FWVs that could generate aerodynamic lift through motions of flapping and achieve lift augmentation through translational flight.

To understand the translational FWVs flight dynamics, we define a *separable model* to be an aerodynamic model which additively separates the thrust generation due to the flapping and translational motion; and an *inseparable model* to be one considering their combined effect. In this paper, we consider the separable model to illustrate the importance of the translational velocity in BFWVs lift generation.

[1] All authors are affiliated to the Elmore Family School of Electrical and Computer engineering at Purdue University.
* is the corresponding author (nhyun@purdue.edu)

In this work, we experimentally validate that some class of BFWV model can not generate sufficient lift through flapping motion alone to achieve hovering. It requires a non-zero translational flight velocity to generate augmented aerodynamic lift forces. A separable nonlinear aerodynamic model is proposed for the cycle-averaged dynamics of BFWV and sufficient conditions on the states of the BFWV are derived so that it could fly with constant speed and orientation.

II. Modeling of Cycle-Averaged BFWV Dynamics

In this section, we model the FWV shown in Fig. 2 as a six DoF translational flyer with the cycle-averaged aerodynamic force directly acting on the body under the following assumptions [19]:

Assumption 1. *The body and wing dynamics are decoupled*

Assumption 2. *The body dynamics depends on the cycle-averaged aerodynamic forces*

Assumptions 1 and 2 are well suited for systems with relatively low-mass wings compared to the body. (e.g., the Harvard RoboBee's wing mass is 1% of the body weight, and the FWV wings shown in Fig. 2 in this paper are 3.5% of the body weight).

Now, suppose that the center of mass (CoM) position is given by $r = (x,y,z)$ in the inertial frame (Fig. 2) where the origin of the body frame is attached to the CoM and aligned with the principal axis of the FWV. Let R_{wb} be the rotation matrix in $SO(3)$ representing the orientation of the vehicle. The coordinates of the system can be represented by $(r,R_{wb}) \in SE(3)$. In addition, let $v \in \mathbb{R}^3$ be the translational velocity in the world frame, and $\omega \in \mathbb{R}^3$ represent the body angular velocity, then the cycle-averaged FWV dynamics is:

$$\dot{r} = v \tag{1}$$
$$\dot{R}_{wb} = R_{wb}\widehat{\omega} \tag{2}$$
$$m\dot{v} = -mge_3 + R_{wb}F_{aero} \tag{3}$$
$$I\dot{\omega} = -\omega \times I\omega + \tau_{aero} \tag{4}$$

where m is the total mass of the vehicle, g is the gravitational acceleration, $F_{aero} \in \mathbb{R}^3$ is the total *cycle-averaged* aerodynamic force acting on the CoM of BFWV's body frame, $\tau_{aero} \in \mathbb{R}^3$ is a vector of *cycle-averaged* torques along the roll, pitch, and yaw axes of BFWV's body frame, and the vector $e_3 = (0,0,1)^\top$ is a unit vector in $\mathbb{R}^3$. Since the body is aligned with the principal axis, the moment of inertia $I \in \mathbb{R}^{3\times3}$ is a diagonal matrix with components (I_{xx},I_{yy},I_{zz}), and $\widehat{\omega}$ is a skew-symmetric matrix such that $\widehat{\omega}y = \omega \times y$ (here, $\times$ indicates a cross product).

Remark 1: Observe that the state $x = (r,R_{wb},v,\omega)$ are the averaged states, and $\overline{F_{aero}}$ and $\overline{\tau_{aero}}$ represent the cycle-averaged aerodynamic model. By averaging the instantaneous aerodynamic forces and torques F_{inst} and τ_{inst} over a flapping cycle, a cycle-averaged model can be obtained.

$$\overline{F}_{aero}(t) = \frac{1}{T}\int_{t-T}^{t} F_{inst}(\tau_1)d\tau_1$$
$$\overline{\tau}_{aero}(t) = \frac{1}{T}\int_{t-T}^{t} \tau_{inst}(\tau_1)d\tau_1$$

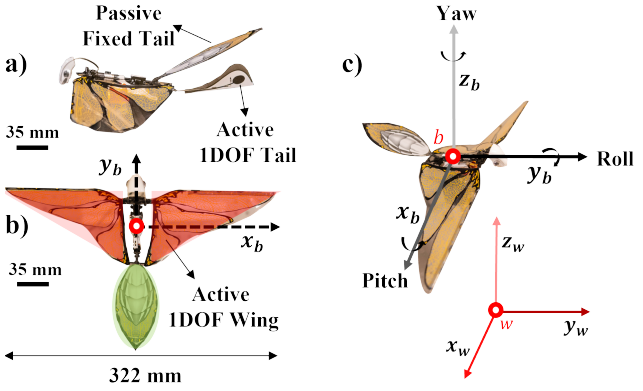

Fig. 2. BFWV side and top view, major aerodynamic loading zones are colored: green represents tail and red represents wings. a) The passive fixed tail can be manually adjusted by applying moment around its hinge; the active 1DoF tail is controlled by a small brushless DC motor. b) The active 1DoF wing is controlled by a bigger brushless DC motor situated at the thorax of the FWV. c) BFWV body-frame axis along with positive Euler angle directions and world frame defined

where F_{inst} and τ_{inst} represent the instantaneous force and torque exerted at the CoM of BFWV.

A. Underactuated BFWV Robot Model

As shown in Fig. 2, a 32cm wing span, bird-scale flapping-wing vehicle weighing 12.0g modified from Bionic Bird [20] is used in this study and it is capable of varying the flapping frequencies from 10 to 14 Hz. Let u_1 and u_2 be the input controls for the wing and the back tail, respectively,

$$u = [u_1,u_2] \in [0,100]$$

which are the duty cycle of each motor. This system is underactuated since it has two inputs (u_1,u_2) which are less than the degrees of freedom (DoF) of the system. Therefore, the cycle-averaged aerodynamic force and torque, $\overline{F_{aero}}$ and $\overline{\tau_{aero}}$ can be defined as a function of these inputs and the averaged states:

$$\overline{F}_{aero}(t) = F_{aero}(u(t),x(t)) \tag{5}$$
$$\overline{\tau}_{aero}(t) = \tau_{aero}(u(t),x(t)). \tag{6}$$

B. Aerodynamic Force Data Acquisition

We have two different ways to measure the aerodynamic forces based on the translational velocity of the flyer. One is a static measurement without translational velocity ($v = 0$), using a 6-axis transducer ATI-Nano17 by mounting the BFWV's CoM to the transducer's reference center of measurement. Three sets of experiments are conducted over each input duty cycles ranging from

$$u_1 \in [70,100]$$

with an increment of 5. Let $F^s_{inst}(t,u) \in \mathbb{R}^3$ and $\tau^s_{inst}(t,u) \in \mathbb{R}^3$ be the measured instantaneous force from the load cell where the superscript s denotes static measurement, then the average aerodynamic force and torque can be obtained by

averaging over n cycles with flapping period T given constant input u_1:

$$\overline{F}_{static}(u_1) = \frac{1}{nT}\sum_{i=1}^{nTf_s} F^s_{inst}(t_1 + (1/f_s)i) \tag{7}$$

$$\overline{\tau}_{static}(u_1) = \frac{1}{nT}\sum_{i=1}^{nTf_s} \tau^s_{inst}(t_1 + (1/f_s)i) \tag{8}$$

where $f_s = 1$ kHz, and t_1 is some initial time. An example of the static instantaneous force data projected on body YZ plane is shown in Fig. 3(a).

Next, we use the motion capture data to obtain the aerodynamic force estimates during the forward flight. The active tracking of the BFWV flight data using motion capture is sampled at $f_t = 150$Hz for an average flight duration of 0.8 seconds (6 cycles). The collected data gives the position and R_{wb} at each time stamp. We can then compute the body angular velocity using the first order approximation on $so(3)$, a skew symmetric matrix, as follows

$$\widehat{\omega}(t) = \frac{\log(R_{wb}(t+\Delta t)R_{wb}(t)^{-1})}{\Delta t} \tag{9}$$

where $\hat{\omega} \in so(3)$ and Δt is the sampling period. BFWV angular velocity ω can then be solved using the definition of the time rate of change of angular rotation:

$$\omega = \left(\frac{\log(R_{wb}(t+\Delta t)R_{wb}(t)^{-1})}{\Delta t}\right)^{\vee}$$

where $\vee$ is the inverse operation of the hat operator. The estimated instantaneous aerodynamic force is then obtained:

$$F^t_{inst}(t) = R^{\top}_{wb}(m\dot{v} + mge_3) \tag{10}$$

$$\tau^t_{inst}(t) = I\dot{\omega} + \omega \times I\omega, \tag{11}$$

where both F^t_{inst} and τ^t_{inst} are force and torque represented on the body frame. An example of the six cycle measurement is shown in Fig. 3(b). Now, by averaging over $n = 6$ flapping cycles, we compute

$$\overline{F}_{aero}(u_1) = \frac{1}{nT}\sum_{i=1}^{nTf_t} F^t_{inst}(t_1 + (1/f_t)i) \tag{12}$$

$$\overline{\tau}_{aero}(u_1) = \frac{1}{nT}\sum_{i=1}^{nTf_s} \tau^t_{inst}(t_1 + (1/f_t)i) \tag{13}$$

for each input u_1 and some initial time t_1.

III. Motivating Example for Insufficient Averaged Lift Force for BFWV to Hover

In this section, we compare two sets of tests operating at the same input duty cycle $u_1 = 80$ in two aerodynamic force data calculation: *Static* and *Translational* aerodynamic forces, $\overline{F}^s_{aero}(u_1)$ and $\overline{F}^t_{aero}(u_1)$, respectively:

1) *Static*: BFWV main motor actuated with a forward translational velocity of $v = 0$ (m/s)
2) *Translational*: BFWV main motor actuated with a forward translational velocity of $v > 0$ (m/s)

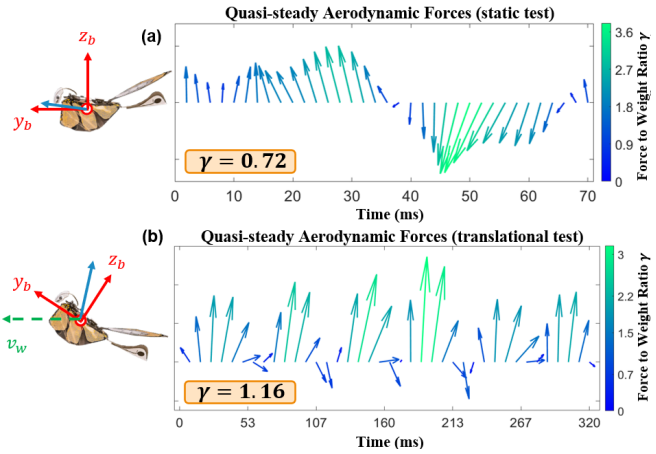

Fig. 3. (a) Quasi-steady force measured during static flight ($v = 0$) projected onto BFWV body YZ plane. (b) Quasi-steady force measured during translational ($v > 0$) projected onto BFWV body YZ plane. Cycle-averaged force vector is shown as blue arrow overlaid with the image of the robot.

We define γ as the normalized cycle-averaged aerodynamic forces over the weight of BFWV as:

$$\gamma = \frac{|\overline{F_{aero}}|}{mg}.$$

The critical value $\gamma \geq 1$ implies that the BFWV is capable of holding altitude during flight since the cycle-averaged lift equals its weight. As shown in Fig. 3(a), $\gamma = 0.72 < 1$ measured over one flapping cycle operating at motor input $u_1 = 80$ (duty cycle) during static flight test indicates that the BFWV can not generate sufficient lift to stay aloft. However, we observe $\gamma = 1.16 > 1$ in Fig. 3(b) during translational flight tests indicating the BFWV flyer can generate enough lift to climb up. Therefore, we postulate that in addition to lift generated through the flapping actuators, there exists lift augmentation during the translational motion. We formally introduce the hybrid notion of lift generation in Section IV and show that the aerodynamic model of the BFWV system described in Equ. (5, 6) can be separable.

IV. Augmented Aerodynamic Force Modeling and System Identification for BFWV

Motivated by the existence of lift augmentation through translational flights previously shown, a separable cycle-averaged aerodynamic model is formally stated as following:

$$\overline{F}_{aero}(u, v, \omega, R_{wb}) = \overline{F}_{static}(u) + \overline{F}_{aug}(v, \Omega, R_{wb}) \tag{14}$$

$$\overline{\tau}_{aero}(u, v, \omega, R_{wb}) = \overline{\tau}_{static}(u) + \overline{\tau}_{aug}(v, \Omega, R_{wb}) \tag{15}$$

where the subscript *static* denotes the aerodynamic forces and torques produced by the BFWV's actuation mechanism through motions of flapping itself; the subscript *aug* denotes the augmented aerodynamic forces and torques produced through the translational motion of the BFWV. Given this separable model, the BFWV dynamics can be formally formulated using the cycle-averaged quasi-steady approach.

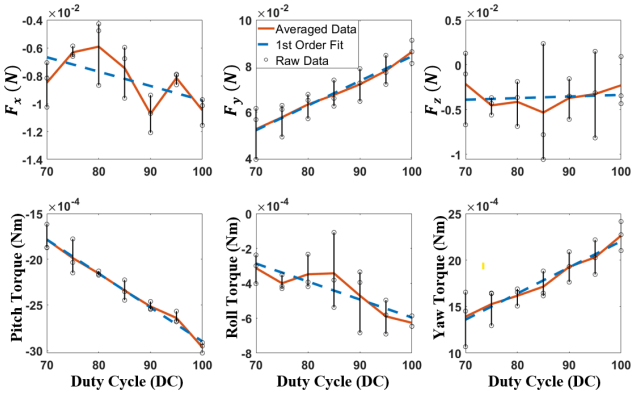

Fig. 4. Static aerodynamic force and torque versus input u; raw data points are shown as error bars, showing three distinct experiments are performed at set duty cycles; linear static model is shown in blue

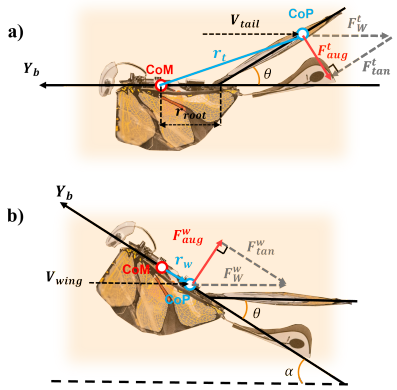

Fig. 5. BFWV force projection schematic showing locations of center of pressure (CoP) on both wing and tail; augmented aerodynamic forces due to translational velocity is shown in red; θ denotes the fixed tail angle relative to body y axis

A. Static Aerodynamic Model and System Identification

The static force data obtained by the 6-axis transducer previously introduced in Section II-B shows the strong linear correlation with the input u_1. A first order approximation for the input duty cycle u_1 to the averaged static aerodynamic force and torque, $\widehat{\overline{F}}_{static}(u_1)$ and $\widehat{\overline{\tau}}_{static}(u_1)$ is proposed:

$$\widehat{\overline{F}}_{static}(u_1) = A_{fs} \cdot u_1 + B_{fs} \tag{16}$$
$$\widehat{\overline{\tau}}_{static}(u_1) = A_{ts} \cdot u_1 + B_{ts} \tag{17}$$

where $A_{fs}, B_{fs}, A_{ts}, B_{ts} \in \mathbb{R}^3$ are unknowns. By formulating the least square error from the static data measurement to the proposed model

$$min_{A_{fs},B_{fs}\in\mathbb{R}^3} \sum_{u_1\in[70,100]} ||\widehat{\overline{F}}_{static}(u_1) - \overline{F}_{static}(u_1)||^2 \tag{18}$$
$$min_{A_{ts},B_{ts}\in\mathbb{R}^3} \sum_{u_1\in[70,100]} ||\widehat{\overline{\tau}}_{static}(u_1) - \overline{\tau}_{static}(u_1)||^2 \tag{19}$$

, we obtain the optimal solutions for A_{fs}, B_{fs}, A_{ts}, and B_{ts}, and the obtained static model is shown in Fig. 4. The static flight test result reveals strong thrust in the body y-axis, and a strong negative pitch torque about the body x-axis.

B. Translational Aerodynamic Model

In this section, we propose a model for augmented aerodynamic forces as a function of the translational velocity, angular velocity, and orientation. First, the following design assumptions are applied:

Assumption 3. *The shear force or skin friction force acting on the wings are negligible.*

Assumption 4. *The BFWV fixed tail is symmetrical in the body XY plane*

The Assumption 3 holds for the wing design with thin film. The BFWV wing membrane shown in Fig. 2 has a thickness of 150 μm, and Assumption 4 is true by its mechanical design. The separable augmented aerodynamic force F_{aug} in Equ. (14) is then modeled with the instantaneous quasi-steady translational aerodynamic model, which depends on the instantaneous state

$$x_r = (v, \omega, R_{wb}), \tag{20}$$

the mean center of pressure location (d), and the lumped aerodynamic constants (K). The unknown constants d and K, which we will formally define in this section, are subject to be learned via system identification.

First, we define the CoP locations of the tail as r_t and of the wing structure (mean CoP between two wings) as r_w, expressed in the body frame, respectively.

$$r_t = \begin{bmatrix} r^t_x & r^t_y & r^t_z \end{bmatrix}^\top$$
$$r_w = \begin{bmatrix} r^w_x & r^w_y & r^w_z \end{bmatrix}^\top$$

Invoking Assumption 4, we assume $r^t_x = 0$ and $r^t_z = -\tan(\theta)(r^t_y + r_{root})$ where θ is the angle shown in Fig. 5(a) and r_{root} defines the distance between CoM to the root of the BFWV tail. Therefore, we denote the unknown CoP locations as design parameters d:

$$d = \begin{bmatrix} r^t_y & r^w_x & r^w_y & r^w_z \end{bmatrix}^\top \tag{21}$$

where $d \in \mathbb{R}^4$ is a vector with non-negative elements.

Next, we define K_t, $K_w \in \mathbb{R}_{\geq 0}$ to be the lumped aerodynamic constant for the tail and wing. By using the velocity-squared dependency between aerodynamic forces and aerodynamic constants [21], F_{aug} can be expressed as a function of K_t and K_w and the velocities at the CoP of the tail and wing. We can express the velocity in the world frame at each CoP on the wing and tail respectively by:

$$V^t_{\mathbb{W}}(x_r, d) = v + R_{wb}\hat{\omega} r_t \tag{22}$$
$$V^w_{\mathbb{W}}(x_r, d) = v + R_{wb}\hat{\omega} r_w \tag{23}$$

where v, ω, and R_{wb} are instantaneous states (cf. not the averaged state as in Equ. (1-4)). Then, the quasi-steady aerodynamic force acting on each wing in the world frame can be formulated as:

$$F^t_{\mathbb{W}} = -K_t |V^t_{\mathbb{W}}| V^t_{\mathbb{W}} \tag{24}$$
$$F^w_{\mathbb{W}} = -K_w |V^w_{\mathbb{W}}| V^w_{\mathbb{W}} \tag{25}$$

From the Assumption 3 and Assumption 4, we define the projection matrix Q_w to extract only the orthogonal component to the mean wing surface, and we define the projection matrix Q_t to project the aerodynamic force on the body YZ plane to remove body X axis aerodynamic force,

$$\begin{aligned} Q_t &= e_3 e_3^\top \\ Q_w &= \left(I_{3\times 3} - e_1 e_1^\top\right) \end{aligned}$$

where e_i is an elementary unit vector. Note that the projection matrix is defined in the body frame, then the aerodynamic forces, F^t_{aug} and F^w_{aug} expressed in the body frame are

$$F^t_{aug} = -K_t ||V^t_{\mathbb{W}}|| Q_t (R^{-1}_{wb} v + \hat{\omega} r_t) \quad (26)$$

$$F^w_{aug} = -K_w ||V^w_{\mathbb{W}}|| Q_w (R^{-1}_{wb} v + \hat{\omega} r_w). \quad (27)$$

The linear force term acting on the system can be modeled by summing the tail and wing contributions, $\widehat{F}_{aug}$. In addition, the induced augmented aerodynamic torque generated by each F^t_{aug} and F^w_{aug} can be computed. Therefore, we have the instantaneous augmented aerodynamic model depending on x_r and the unknown parameters (d,K):

$$\widehat{F}_{aug}(x_r,d,K) = A(x_r,d)\cdot K_t + B(x_r,d)\cdot K_w \quad (28)$$

$$\widehat{\tau}_{aug}(x_r,d,K) = C(x_r,d)\cdot K_t + D(x_r,d)\cdot K_w \quad (29)$$

where $A(x_r,d), B(x_r,d), C(x_r,d)$, and $D(x_r,d) \in \mathbb{R}^3$ are defined as:

$$\begin{aligned} A(x_r,d) &:= -||V^t_{\mathbb{W}}|| Q_t (R^{-1}_{wb} v + \hat{\omega} r_t) \\ B(x_r,d) &:= -||V^w_{\mathbb{W}}|| Q_w (R^{-1}_{wb} v + \hat{\omega} r_w) \\ C(x_r,d) &:= \hat{r}_t F^t_{aug} \\ D(x_r,d) &:= \hat{r}_w F^w_{aug}. \end{aligned}$$

Remark 2: Observe that the aerodynamic constants K has linear dependency in the model but the unknown CoP parameters d appears non-linearly due to the square dependency of the $V^t_{\mathbb{W}}$ and $V^w_{\mathbb{W}}$. We exploit this structure in the system identification in the next section.

C. Nonlinear System Identification for Augmented Aerodynamic Force

In this section, we first aim to learn the unknown parameters d and K in the augmentation model Equ. (28-29). Let the cycle-averaged augmentation error to be defined as

$$\bar{y}(u_1) = \begin{bmatrix} \overline{F}_{aero}(u_1) - \widehat{\overline{F}}_{static}(u_1) \\ \overline{\tau}_{aero}(u_1) - \widehat{\overline{\tau}}_{static}(u_1) \end{bmatrix} \quad (30)$$

where $\bar{y}(u_1) \in \mathbb{R}^6$ and $\overline{F}_{aero}(u_1), \overline{\tau}_{aero}(u_1)$ are obtained from the open-loop experiment mentioned in Section II-B, and $\widehat{\overline{F}}_{static}(u_1), \widehat{\overline{\tau}}_{static}(u_1)$ are obtained from the identified model in Sec IV-A.

Each open-loop experiment, we obtain instantaneous state $x_r = (v, \omega, R_{wb})$ (c.f, not the cycle-averaged state), and we compute the predicted averaged force from the model in Equ. (28-29),

$$\widehat{\bar{y}}(u_1,d,K) = \frac{1}{nT}\sum_{i=1}^{nTf_t} \begin{bmatrix} \widehat{F}_{aug}(x_r(t_1+(1/f_s)i),d,K) \\ \widehat{\tau}_{aug}(x_r(t_1+(1/f_s)i),d,K) \end{bmatrix} \quad (31)$$

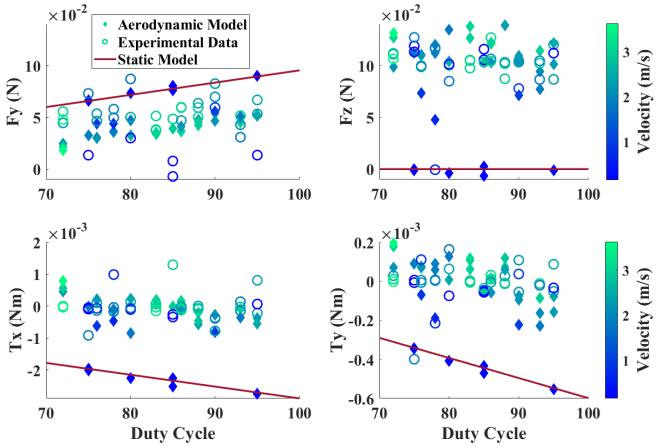

Fig. 6. Proposed separable reduced-order aerodynamic model in comparison with experimental and static aerodynamic forces and torques measurements; existence of lift augmentation in F_z due to BFWV's non-zero translational velocity is shown.

where $\widehat{\bar{y}} \in \mathbb{R}^6$. Since K appears linearly in Equ. (28-29), we can formulate $\widehat{\bar{y}}(u_1,d,K)$ as

$$\widehat{\bar{y}}(u_1,d,K) = \overline{G}(d)K \quad (32)$$

for some $\overline{G}(d) \in \mathbb{R}^{6\times 2}$ derived from Equ. (28-29). Then, we can derive the analytic optimal solution for K which minimizes the constrained weighted least square constrained optimization problem:

$$K^*(d) := \arg\min_K \frac{1}{2}(\bar{\bar{y}} - \overline{G}(d)\cdot K)^T W (y - \overline{G}(d)\cdot K) \quad (33)$$

subject to $K_t, K_w > 0$.
The Hamiltonian of the system with two Lagrange multipliers $\lambda = (\lambda_1, \lambda_2)^\top \in \mathbb{R}^2$ is defined as

$$H = \frac{1}{2}(\bar{\bar{y}} - \overline{G}(d)\cdot K)^T W (y - \overline{G}(d)\cdot K) - \lambda_1 K_t - \lambda_2 K_w \quad (34)$$

and by considering necessary conditions for the stationary solution, we have

$$K^*(d,\lambda) = (\overline{G}(d)^T W \overline{G}(d))^{-1} \overline{G}(d)^T W \bar{\bar{y}} + (\overline{G}(d)^T W \overline{G}(d))^{-1} \lambda \quad (35)$$

where $\lambda_1, \lambda_2 > 0$, satisfying the Karush–Kuhn–Tucker (KKT) conditions.

Now, by substituting the optimal K^* back into the weighted cost function in Equ. (33), we formulate the nonlinear optimization problem with d as the only parameters:

$$d^* = \arg\min_{d\in U_d} \frac{1}{2}(\bar{\bar{y}} - \overline{G}(d)\cdot K^*(d))^T W (y - \overline{G}(d)\cdot K^*(d)) \quad (36)$$

subject to

$$\lambda_1 > 0 \wedge \lambda_2 > 0 \wedge d \in U_d$$

where $\wedge$ is the logical AND operation, and U_d is the bounds for CoP location given the geometry of the robot shown in Fig. 2. Finally, this problem is solved with the NLP solver in MATLAB using the interior-point-method.

Once we find the d^* numerically, we compute for the corresponding optimal $K^*(d^*)$ using Equ. (35). This procedure is repeated for every $N = 39$ open-loop experiment described in Sec II-B. By collecting all $K^*(i), d^*(i)$ optimal solutions for each experiment, the averaged $\overline{K}$ and $\overline{d}$ are obtained by

$$\overline{K} = \frac{1}{N}K^*(i),\ \overline{d} = \frac{1}{N}d^*(i)$$

Finally, the cycle-averaged separable aerodynamic model is defined as

$$\widehat{\overline{F}}_{aero}(u_1, \bar{x}_r) = \widehat{\overline{F}}_{static}(u_1) + \widehat{\overline{F}}_{aug}(\bar{x}_r, \overline{d}, \overline{K}) \quad (37)$$

$$\widehat{\overline{\tau}}_{aero}(u_1, \bar{x}_r) = \widehat{\overline{\tau}}_{static}(u_1) + \widehat{\overline{\tau}}_{aug}(\bar{x}_r, \overline{d}, \overline{K}) \quad (38)$$

where x_r is the averaged state and all proposed model with $\widehat{[\,]}$ are from Equ. (16-17) and Equ. (28-29).

Remark 3: The results of the proposed model is shown in Fig. 6. This model is obtained using the flight data in the velocity range of $v = [2.63, 3.62]$ m/s. The experimentally obtained force data and the predicted model show a strong match and correlation at the higher translational velocities (green, $v > 2$m/s). The predicted model at lower translational velocities (blue, $v < 2$m/s) corresponds well to the static model (solid red line) as expected. Overall, the proposed model indicates the presence of significant aerodynamic force augmentation during BFWV's higher velocity flights.

V. Analysis of BFWV Dynamics and Feasible Trajectories

In this section, the feasible trajectory of the BFWV model using the proposed cycle-averaged separable aerodynamic model will be analyzed. First, the cycle-averaged reduced order model (removing the position kinematics from Equ. (1-4) using the can be defined as

$$\dot{R_{wb}} = R_{wb}\hat{\omega} \quad (39)$$

$$m\dot{v} = -mge_3 + R_{wb}\widehat{\overline{F}}_{aero}(u_1, \bar{x}_r) \quad (40)$$

$$I\dot{\omega} = -\omega \times I\omega + \widehat{\overline{\tau}}_{aero}(u_1, \bar{x}_r) + \tau_z(u_2)e_3 \quad (41)$$

where $x_r = (R_{wb}, v, \omega)$ and $\widehat{\overline{F}}_{aero}(u_1, \bar{x}_r), \widehat{\overline{\tau}}_{aero}(u_1, \bar{x}_r)$ are from Equ. (37-38). We hypothesize that the tail control u_2 can generate direct yaw torque to the system. The system identification of the yaw torque will be further conducted in the future. In this section, we aim for generating the possible trajectory from the given aerodynamic model when the yaw torque can be controlled separately.

A. A Set of Equilibrium of the Reduced Order Model

Suppose that a set S is a collection of stationary points of the reduced order dynamics, then

$$S := \{x \in SE(3) \mid \exists u \in U s.t. \omega = 0 \wedge \dot{\omega} = 0 \wedge \dot{v} = 0\}$$

where U is the input bound. Note that $\omega = 0$ if and only if $\dot{R}_{wb} = 0$. In particular, we are interested in the forward flight, meaning that the lateral velocity of the body x axis is zero, namely $e_1^\top R_{wb}^\top v = 0$. Therefore we consider a subset of S:

$$E := \{x \in S \mid e_1^\top R_{wb}^\top v = 0\},$$

and the next theorem shows the existence of an equilibrium and a control input u such that this set is non-empty.

First, let the following constant matrix and vectors be defined as:

$$J := \begin{bmatrix} 0 & 0 \\ 1 & 0 \\ 0 & 1 \end{bmatrix} \qquad L := \begin{bmatrix} 1 & 0 & 0 \\ 0 & 1 & 0 \end{bmatrix}$$

$$P := -(K_t\widehat{r_t}Q_t + K_w\widehat{r_w}Q_w) \quad \overline{P} := L \cdot P$$

$$\overline{\overline{P}} := L \cdot P \cdot J \qquad \overline{\alpha} := A_{fs} - P_x J\overline{\overline{P}}^{-1}\overline{A_{ts}}$$

$$P_x := Q_t K_t + Q_w K_w \quad \overline{\beta} := P_x J\overline{\overline{P}}^{-1}\overline{B_{ts}} - B_{fs}$$

Theorem 1. *If there exist u_1, v, R_{wb} such that they satisfy the following conditions:*

$$||v||v = R_{wb}J\overline{\overline{P}}^{-1}(\overline{A_{ts}}u_1 + \overline{B_{ts}}) \quad (42)$$

$$\overline{\alpha}u_1 = R_{wb}^T e_3 mg + \overline{\beta} \quad (43)$$

then the set E is nonempty.

Proof: If $u \in U$ is the control such that it makes $x_r = (R_{wv}, v, 0_{3\times 1}) \in S$, then $\dot{v} = 0$ and $\dot{\omega} = 0$ using the same u. Therefore, it is enough to show that there indeed exists such u. By imposing this u and making $\dot{\omega} = 0$:

$$A_{ts}u_1 = P||v_b||\top v_b - B_{ts} - \tau_z e_3 \quad (44)$$

where $v_b = R_{wb}^\top v$, $P \in \mathbb{R}^{3\times 3}$ is a constant upper triangular matrix (with nonzero elements), and v_b is the body frame velocity. Observe that $e_3^\top P = 0$ since the augmented aerodynamic force projecting on body YZ plane does not generate any yaw torque.

By setting the yaw control $\tau_z(u_2)$ to be

$$\tau_z = -e_3^T A_{ts}u_1 - e_3^T B_{ts} \quad (45)$$

for any u_1, we have $e_3^\top \dot{\omega} = 0$.

Therefore, we need to find the necessary condition for (u_1, v, R_{wb}) such that $e_1^\top \dot{\omega} = e_2^\top \dot{\omega} = 0$, which simplifies the condition in Equ. (44) to

$$\overline{P}||v_b||v_b = \overline{A_{ts}}u_1 + \overline{B_{ts}}. \quad (46)$$

Observe that since $Pe_1 = 0_{3\times 1}$, we can rewrite Equ. (46) and back out the first sufficient condition:

$$||v_b||v_b = J\overline{\overline{P}}^{-1}(\overline{A_{ts}}u_1 + \overline{B_{ts}}) \quad (47)$$

$$||v||v = R_{wb}J\overline{\overline{P}}^{-1}(\overline{A_{ts}}u_1 + \overline{B_{ts}})$$

The implicit condition between u_1 and v_b in Equ. (47) with the yaw torque control in Equ. (45) guarantees that $\dot{w} = 0$. By using the definition for $v = R_{wb}v_b$ and apply to the assumption stated in the theorem, Equ. (42), we know that there exist v_b and u_1 satisfying Equ. (47) to ensure $\dot{w} = 0$. Furthermore, $e_1^\top R_{wb}^\top v = 0$ holds for v satisfying (47) since $e_1^\top J = 0_{1\times 2}$.

Now, we need to ensure that the choice of u_1 and v_b also guarantee the condition $\dot{v} = 0$. The sufficient condition for $\dot{v} = 0$ thus gives:

$$A_{fs}u_1 = P_x||v_b||v_b - B_{fs} + R_{wb}^T e_3 mg.$$

By substituting $||v_b||v_b$ from Equ. (47) as a function of u_1 we obtain the second sufficient condition:

$$\overline{\alpha}u_1 = R_{wb}^T e_3 mg + \overline{\beta} \tag{48}$$

From the assumption of the theorem, there exists such u_1 and R_{wb} satisfying the above two conditions. Hence, the two sufficient conditions in Equ. (42-43) guarantees the existence of control u such that E is not empty. □

B. Numerical Verification

Using the identified parameters for $\overline{d}, \overline{K}$ in Sec IV-C, we compute the required control u_1 to achieve a stable translational flight with zero angular moment. A numerical constrained optimization problem is formulated and solved to find u_1 and R_{wb}:

$$(u_1^*, \Gamma^*) = \underset{u_1,\Gamma}{\arg\min}(||\overline{\alpha}u_1 - \overline{\beta} - \Gamma mg||^2 \tag{49}$$

subject to

$$\underline{u_1} \leq u_1 \leq \overline{u_1}, \quad ||\Gamma||^2 = 1,$$

where Γ represents $R_{wb}^T e3$ the world-frame z axis in the body-frame and the lower and upper bounds for u are defined as $\underline{u_1} = 40$ and $\overline{u_1} = 100$. Once the solution is obtained, there is one degree of freedom to construct the full R_{wb} by taking orthogonal components to Γ^*, and using the cross product to generate the third axis while ensuring $det(R_{wb}) = 1$. Next, using R_{wb} and u_1, we compute v using Equ. (42). The numerical solution shows that

$$u_1 = 76.25$$

$$\tau_z = -1.5 \quad Nmm$$

$$v_b = \begin{bmatrix} 0 & 2.73 & -1.482 \end{bmatrix}^T$$

$$R_{wb} = \begin{bmatrix} 0.9245 & -0.3274 & 0.1952 \\ 0.3738 & 0.8790 & -0.2961 \\ -0.0746 & 0.3467 & 0.9350 \end{bmatrix}$$

Based on the sufficient conditions shown above, we conclude that in order for the BFWV to perform straight-line flight at a constant velocity with zero angular moments, it is necessary for $v_b^z < 0$ which allows it to increase its total aerodynamic lift matching its body weight through the lift augmentation method proposed in Section IV. Therefore, the current solution indicates that the BFWV can not maintain a constant altitude flight. However, an oscillatory flight trajectory over a fixed altitude could be a possible solution, which we observe during the manually-controlled flight tests.

VI. Conclusion and Future Work

From experimental testing and preliminary analysis of the BFWV flights, we observe that the BFWV may require augmented lift generated through translational motion to remain aloft. A velocity-dependent aerodynamic model is formally proposed by defining a cycle-averaged BFWV dynamical model using system-identification and it is shown that the proposed model could validate the existence of lift augmentation through non-zero translational velocity during forward flights. By analyzing the stationary points of the BFWV dynamics, it is shown that a negative z velocity in its body frame (e.g., in the form of wind or flying with a positive pitch angle) is required for it to achieve sufficient lift to stay aloft. In future, tail dynamics could be incorporated into our current model, and demonstrate the full feedback controlled flight of the underactuated BFWV flyer.

References

[1] K. Y. Ma, S. M. Felton, and R. J. Wood, "Design, fabrication, and modeling of the split actuator microrobotic bee," in *IEEE/RSJ Intl. Conf. Intell. Robots and Syst. (IROS)*, 2012, pp. 1133–1140.

[2] Y. Chukewad and S. Fuller, "Yaw control of a hovering flapping-wing aerial vehicle with a passive wing hinge," *IEEE Robot. Autom. Lett.*, vol. 6, no. 2, pp. 1864–1871, 2021.

[3] Z. Tu, F. Fei, J. Zhang, and X. Deng, "An at-scale tailless flapping-wing hummingbird robot. i. design, optimization, and experimental validation," *IEEE Trans. Robot.*, vol. 36, no. 5, pp. 1511–1525, 2020.

[4] X. Fang, Y. Wen, Z. Gao, K. Gao, Q. Luo, H. Peng, and R. Du, "Review of the flight control method of a bird-like flapping-wing air vehicle," *Micromachines*, vol. 14, no. 8, p. 1547, 2023.

[5] H.-Y. Kim, J.-S. Lee, H.-L. Choi, and J.-H. Han, "Autonomous formation flight of multiple flapping-wing flying vehicles using motion capture system," *Aerospace Science and Technology*, vol. 39, pp. 596–604, 2014.

[6] H. Xu, E. Pan, D. Xue, W. Xu, Y. Wang, and X. Liang, "An aerodynamics calculation method of a flapping wing flying robot based on state-space airloads theory," in *2019 IEEE(ROBIO)*. IEEE, 2019, pp. 1821–1826.

[7] W. Yang, L. Wang, and B. Song, "Dove: A biomimetic flapping-wing micro air vehicle," *International Journal of Micro Air Vehicles*, vol. 10, no. 1, pp. 70–84, 2018.

[8] H. Huang, W. He, J. Wang, L. Zhang, and Q. Fu, "An all servo-driven bird-like flapping-wing aerial robot capable of autonomous flight," *IEEE/ASME Transactions on Mechatronics*, vol. 27, no. 6, pp. 5484–5494, 2022.

[9] H. A. Bruck and S. K. Gupta, "A retrospective of project robo raven: Developing new capabilities for enhancing the performance of flapping wing aerial vehicles," *Biomimetics*, vol. 8, no. 6, 2023.

[10] R. Meng, B. Song, J. Xuan, and X. Yang, "Design and verification of a large-scaled flapping-wing aircraft named "cloud owl"," *Applied Sciences*, vol. 13, no. 9, 2023.

[11] A. T. Pfeiffer, J.-S. Lee, J.-H. Han, and H. Baier, "Ornithopter flight simulation based on flexible multi-body dynamics," *Journal of Bionic Engineering*, vol. 7, no. 1, pp. 102–111, 2010.

[12] S. Pourtakdoust and S. K. Aliabadi, "Evaluation of flapping wing propulsion based on a new experimentally validated aeroelastic model," *Scientia Iranica*, vol. 19, no. 3, pp. 472–482, 2012.

[13] B.-J. Tsai and Y.-C. Fu, "Design and aerodynamic analysis of a flapping-wing micro aerial vehicle," *Aerospace Science and Technology*, vol. 13, no. 7, pp. 383–392, 2009.

[14] S. F. Armanini, J. V. Caetano, G. C. H. E. de Croon, C. C. de Visser, and M. Mulder, "Quasi-steady aerodynamic model of clap-and-fling flapping mav and validation using free-flight data," *Bioinspiration & Biomimetics*, vol. 11, no. 4, p. 046002, jun 2016.

[15] J. H. Park and K.-J. Yoon, "Designing a biomimetic ornithopter capable of sustained and controlled flight," *Journal of Bionic Engineering*, vol. 5, no. 1, pp. 39–47, 2008.

[16] C. J. Pennycuick, "Power requirements for horizontal flight in the pigeon *Columba Livia*," *Journal of Experimental Biology*, vol. 49, no. 3, pp. 527–555, 1968.

[17] C. P. Ellington, C. Van Den Berg, A. P. Willmott, and A. L. R. Thomas, "Leading-edge vortices in insect flight," *Nature*, vol. 384, no. 6610, pp. 626–630, 1996.

[18] Y.-H. J. Fei and J.-T. Yang, "Enhanced thrust and speed revealed in the forward flight of a butterfly with transient body translation," *Physical Review E*, vol. 92, no. 3, p. 033004, 2015.

[19] K. Y. Ma, P. Chirarattananon, S. B. Fuller, and R. J. Wood, "Controlled flight of a biologically inspired, insect-scale robot," *Science*, vol. 340, no. 6132, pp. 603–607, 2013.

[20] E. V. Ruymbeke. Bionic bird: Metafly.

[21] Anderson, *Fundamentals of aerodynamics*, 6th ed. McGraw-Hill Education, 2024.